Chapter 5
Bremsstrahlung of Fast Charged Particles in a Solid Body

5.1 Polarization Bremsstrahlung in a Single Crystal

5.1.1 General Expression for the Cross-Section of a Radiative Process on an Atomic Ensemble

The cross-section of a photoprocess on an atomic ensemble (in case of a monatomic target) can be represented in the following form [1]:

$$d\sigma_{target} = \left| \sum_j \exp\left(i\,\mathbf{q}\,\mathbf{r}_j\right) \right|^2 d\sigma_{atom}, \tag{5.1}$$

where summation is performed over all atoms of the target being in the volume of interaction, $d\sigma_{atom}$ is the differential cross-section of the process on one atom under consideration,

$$\mathbf{q} = \left(\mathbf{p}_f - \mathbf{p}_i\right)/\hbar + \mathbf{k}$$

is the wave vector transferred from an incident particle (IP) to the target, $\mathbf{p}_i$, $\mathbf{p}_f$ are the initial and final momenta of the IP, $\mathbf{k}$ is the wave vector of a photon. For a substance consisting of atoms of different kinds the formula (5.1) is obviously generalized.

The expressions for the cross-sections of bremsstrahlung of fast charged particles on an atom are given in Chap. 2 both for the static channel (see the formulas (2.43), (2.45)) and for the polarization channel (see Eqs. 2.42 and 2.50).

In the state of thermodynamic equilibrium the squared absolute value in the formula (5.1) should be correspondingly averaged:

V. Astapenko, *Polarization Bremsstrahlung on Atoms, Plasmas, Nanostructures and Solids*, Springer Series on Atomic, Optical, and Plasma Physics 72,
DOI 10.1007/978-3-642-34082-6_5, © Springer-Verlag Berlin Heidelberg 2013

$$\left|\sum_j \exp\left(i\,\mathbf{q}\,\mathbf{r}_j\right)\right|^2 \rightarrow \left\langle \sum_{j,\,j'} \exp\left(i\,\mathbf{q}\,\left(\mathbf{r}_j - \mathbf{r}_{j'}\right)\right)\right\rangle. \tag{5.2}$$

The angle brackets on the right side of the Eq. 5.2 imply thermodynamic averaging.

5.1.2 Structure Factor of a Three-Dimensional Crystal

The structure factor of a medium in a three-dimensional case (a three-dimensional single crystal, the angle brackets mean averaging over atomic positions) is [1]:

$$\left\langle \sum_{j,j'} \exp\left(i\,\mathbf{q}\,\left(\mathbf{r}_j - \mathbf{r}_{j'}\right)\right)\right\rangle = N\left(1 - \exp\left(-u^2\,q^2\right)\right) + N\,n_a\,(2\pi)^3 \sum_{\mathbf{g}} e^{-u^2\,g^2}\,|S(\mathbf{g})|^2\,\delta^{(3)}(\mathbf{q}-\mathbf{g}), \tag{5.3}$$

where $N = N_0\,N_{cell}$ is the full number of atoms in the volume of interaction, N_0 is the full number of cells in the volume of interaction, N_{cell} is the number of atoms in a unit cell, $\mathbf{g}$ is the wave vector of a reciprocal lattice, $n_a = N_{cell}/\Delta_{cell}$ is the volume concentration of atoms, Δ_{cell} is the volume of a unit cell.

In the formula (5.3) the value $S(\mathbf{q})$ is introduced – the *normalized* structure factor of a unit cell of a crystal on the wave vector q, $S(\mathbf{q}=0) = 1$, $\delta^{(3)}(\mathbf{q}) = \delta(q_x)\,\delta\left(q_y\right)\,\delta(q_z)$ is the three-dimensional delta function of the wave vector transferred to the target.

The first summand on the right side of the equation (5.3) describes incoherent scattering of an electromagnetic field by the atoms of a lattice. It is proportional to the number of atoms in the volume of interaction in the first degree. The second summand on the right side of (5.3) describes coherent scattering proportional to the squared concentration of atoms since $N = n_a\,V$.

As can be seen from the formula (5.3), coherent scattering takes place only when a wave vector transferred to a medium is equal to the reciprocal lattice vector $\mathbf{q} = \mathbf{g}$. Formally this circumstance manifests itself as the presence of delta functions in the coherent term. From the formula (5.3) it follows that in the limit of high transferred momenta, when $u^2\,q^2 > 1$, the incoherent component of the structure factor of the medium prevails. In case of fulfilment of the opposite inequation, the main contribution to the process is made by the coherent part of the structure factor of (5.3).

For a face-centered cubic lattice that corresponds to a number of metals such as aluminum, iron, copper, silver, and gold, the geometrical structure factor of a unit cell is equal to [2]:

$$S(\mathbf{g}) = \frac{1}{4}[1 + \cos[\pi\,(n_1 + n_2)] + \cos[\pi\,(n_3 + n_2)] + \cos[\pi\,(n_1 + n_3)]], \tag{5.4}$$

where $\mathbf{g} = n_1\,\mathbf{b}_1 + n_2\,\mathbf{b}_2 + n_3\,\mathbf{b}_3$; $\mathbf{b}_1,\ \mathbf{b}_2,\ \mathbf{b}_3$ are the basis vectors of the reciprocal lattice; $n_1,\ n_2,\ n_3$ are the integers. In case of a lattice *with the diamond structure* that silicon and germanium also have, instead of (5.4) we have:

$$S(\mathbf{g}) = \frac{1}{4}\cos\left[\frac{\pi}{4}\,(n_1 + n_2 + n_3)\right] \times [1 + \cos[\pi\,(n_1 + n_2)] + \cos[\pi\,(n_3 + n_2)] + \cos[\pi\,(n_1 + n_3)]]. \tag{5.5}$$

5.1.3 Cross-Section and Yield of Bremsstrahlung Photons

For convenience of comparison with an experiment, it is advisable to go from the cross-section of Bs on an atom to the differential yield of a number of photons per unit crystal length to the unit solid angle and in the unit frequency range:

$$\frac{dN}{d\omega\,d\Omega_{\mathbf{n}}\,dx} = \frac{d\sigma}{V\,d\omega\,d\Omega_{\mathbf{n}}}, \tag{5.6}$$

where V is the volume of interaction, N is the number of bremsstrahlung photons.

Hence with the use of the following formula

$$\frac{d\sigma_{ii}^{pol}}{d\omega\,d\Omega_{\mathbf{k}}} = \frac{2\,e_0^2\,\left|\,\omega^2\,\alpha_i(\omega)\right|^2}{\pi\,\mathrm{v}^2\,\mathrm{c}^3\,\hbar\omega}\int\limits_{q_{\min}}^{q_{\max}} I_\varphi(q,\mathrm{v},\omega,\theta)\,\tilde{F}_i^2(q)\,\frac{dq}{q} \tag{5.7}$$

for the cross-section of PBs on an atom, where the integral $I_\varphi(q,\mathrm{v},\omega,\theta)$ is given by the Eq. 4.53, in view of the coherent part of the structure factor of the medium (Eq. 5.3), the following expression can be obtained for the coherent part of PBs in a single crystal in case of a *nonrelativistic* incident electron (a nonrelativistic electron is considered here for simplicity of the formulas):

$$\frac{dN_{PB}^{(coh)}}{dx\,d\omega\,d\Omega_{\mathbf{k}}} = \frac{n_a^2\,e^2}{\pi\hbar\,\mathrm{v}\,c^3}\sum_{\mathbf{g}} S^2(\mathbf{g})\,\delta(\omega + \mathbf{g}\mathbf{v} - \mathbf{k}\mathbf{v})\,\omega^3\,|\alpha(\omega)|^2\,\exp\left(-u^2\,g^2\right)\tilde{F}_a^2(g)\,\frac{[\mathbf{s},\mathbf{g}]^2}{\mathbf{g}^4}, \tag{5.8}$$

where $\mathbf{s}$ is the unit vector in the direction of propagation of a photon, $\tilde{F}_a$ is the normalized form factor of a medium atom. The delta function appearing on the right side of this equation gives the relation between the frequency and the angle of

photon emission $\theta = \mathbf{v}\hat{}\mathbf{k}$ for the specified reciprocal lattice vector $\mathbf{g}$. As a result, the relationship is true:

$$\omega = -\frac{\mathbf{g}\,\mathbf{v}}{1 - \frac{\mathrm{v}}{c}\cos\theta}. \tag{5.9}$$

Here for generality the term with the ratio v/c in the denominator is retained.

The relation (5.9) defines the frequency-angular distribution of coherent PBs in scattering of a charged particle in a three-dimensional single crystal.

In the geometry of the process shown in Fig. 5.1 for the frequency of coherent PBs from the formula (5.9) we have in the nonrelativistic limit:

$$\omega_{\mathbf{g}} = \frac{2\pi\,\mathrm{v}}{d}\,[n_1\,\cos\alpha - \sin\alpha\,(n_2\,\cos\phi + n_3\,\sin\phi)], \tag{5.9a}$$

d is the crystal lattice constant, $n_1,\ n_2,\ n_3$ are the integers specifying the reciprocal lattice vector.

In the high-frequency spectral range, when $\alpha(\omega) \to -Z\,e^2/m\,\omega^2$, the expression for coherent PBs in a single crystal (Eq. 5.8) passes into the formula for X-ray parametric radiation [1].

With the use of the incoherent component of the structure factor of the crystal (Eq. 5.3) the incoherent part of PBs can be obtained. As a result, for the frequency-angular distribution of photon yield per unit trajectory length we have for a nonrelativistic incident electron:

$$\frac{dN_{pol}^{(incoh)}}{d\omega\,d\Omega_{\mathbf{k}}\,dx} = n_a\,\frac{e^2}{\hbar\,\omega}\,\frac{\left|\omega^2\alpha(\omega)\right|^2}{\pi\,\mathrm{v}^2\,c^3} \times \left(1 + \cos^2\theta\right)\int\limits_{q_{\min}}^{q_{\max}} \left(1 - \exp\left(-u^2\,q^2\right)\right)\tilde{F}_a^2(q)\ \frac{dq}{q}, \tag{5.10}$$

where $q_{\min} \simeq \omega/\mathrm{v}$, $q_{\max} = 2m\,\mathrm{v}/\hbar$ are the minimum and maximum wave vectors transferred from an incident electron to the medium.

Given in Fig. 5.2 are the intensities of different channels of PBs of an electron with a velocity of $1.5{\cdot}10^9$ cm/s scattered in a silicon single crystal as functions of the input angle α for $\varphi = \pi$ (see the definitions of the angles α and φ in Fig. 5.1). In Fig. 5.2 the solid curve represents coherent PBs; the dotted curve is for coherent PBs calculated with the high-frequency polarizability of atoms; the dashed curve is for incoherent PBs averaged over frequency with a relative resolution of 0.3 %.

It is seen that the intensity of coherent PBs calculated with the high-frequency polarizability $\alpha(\omega) = -Z\,e^2/m\,\omega^2$ does not depend on the angle of electron incoming into a single crystal. This circumstance is explained by the fact that in the high-frequency limit the polarization charge number proportional to $\left|\omega^2\alpha(\omega)\right|$

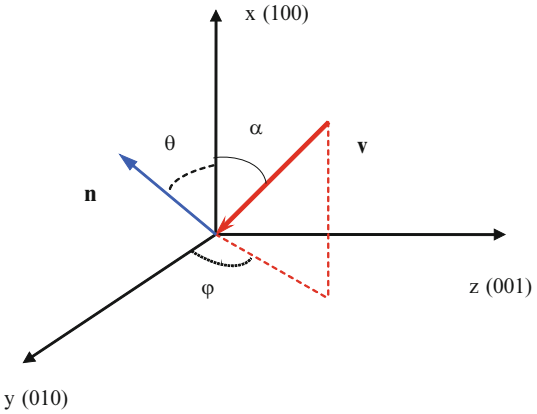

Fig. 5.1 The geometry of PBs in a single crystal

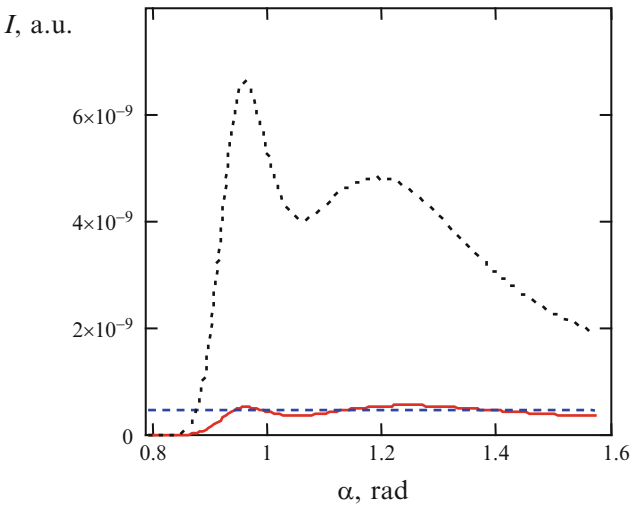

Fig. 5.2 The intensity of PBs of a nonrelativistic electron in a silicon single crystal as a function of the input angle (see the text)

does not depend on the radiation frequency. In calculation of the curves shown in Fig. 5.2 the contribution of 4-vectors of the reciprocal crystal lattice giving the identical dependence of radiation frequency on the input angle according to the Eq. 5.9 was taken into account.

Let us give here also the expressions describing total Bs of a *nonrelativistic* electron in a single crystal in view of the polarization and ordinary channels. For the coherent component of photon yield per unit trajectory length we have:

$$\frac{dN_{tot}^{(coh)}}{d\omega\, d\Omega_{\mathbf{k}}\, dx} = \frac{n_a^2\, Z^2 e^6}{\pi\, \hbar\omega\, \mathrm{v}\, m^2\, c^3} \times$$
$$\times \sum_{\mathbf{g}} S^2(\mathbf{g})\ \delta(\omega + \mathbf{gv} - \mathbf{kv}) \exp\left(-u^2\, g^2\right)$$
$$\times \left| 1 - \tilde{F}_a(q) - \frac{m\,\omega^2}{Z\, e^2}\, \alpha(\omega)\, \tilde{F}_a(g) \right|^2 \frac{[\mathbf{s}, \mathbf{g}]^2}{\mathbf{g}^4}. \qquad (5.11)$$

The incoherent component of total Bs of an electron is:

$$\frac{dN_{tot}^{(incoh)}}{d\omega\, d\Omega_{\mathbf{k}}\, dx} = n_a\, \frac{Z^2 e^6}{\hbar\,\omega}\, \frac{(1 + \cos^2\theta)}{\pi\, \mathrm{v}^2\, m^2\, c^3} \int_{q_{\min}}^{q_{\max}} \left(1 - \exp\left(-u^2\ q^2\right)\right)$$
$$\times \left| 1 - \tilde{F}_a(q) - \frac{m\,\omega^2}{Z\, e^2}\, \alpha(\omega)\, \tilde{F}_a(q) \right|^2 \frac{dq}{q}. \qquad (5.12)$$

On the right side of the Eqs. 5.11 and 5.12 the first two summands under the modulus sign describe the contribution of ordinary Bs to the process, and the third summand corresponds to PBs.

It should be noted that the coherent and incoherent components of bremsstrahlung do not interfere with each other.

From the formulas (5.11) and (5.12) it follows that in the high-frequency limit ($\alpha(\omega) \to -Z\, e^2/m\,\omega^2$) the second and third summands under the modulus sign cancel out, which corresponds to the *descreening effect* (or the effect of atom "stripping") in the process of Bs. It should be noted that this effect takes place only for a nonrelativistic incident electron.

For relativistic electrons in the most part of the spectral range the main contribution to the process is made by the coherent component of Bs, when the momentum excess from an incident particle is transferred to the crystal lattice as a whole. In the nonrelativistic case, generally speaking, the contributions of the coherent and incoherent Bs channels are comparable in value.

5.2 Polarization Bremsstrahlung in a Polycrystal

Serving as initial expressions for calculation of PBs of a fast charged particle in a polycrystal are the formulas (5.8) and (5.9). Going from a single crystal to a polycrystal consists in averaging the expression for the coherent component of PBs (5.8) over the solid angle of the reciprocal lattice vectors $\Omega_{\mathbf{g}}$ according to the equation

$$\left(\frac{dN}{d\omega\, d\Omega_{\mathbf{k}}\, dx}\right)_{polycr} = \int \frac{dN}{d\omega\, d\Omega_{\mathbf{k}}\, dx}\, \frac{d\Omega_{\mathbf{g}}}{4\,\pi}. \qquad (5.13)$$

It is obvious that such an averaging for the incoherent component of PBs (5.10) will not change the initial expression that does not depend on the vectors of the reciprocal lattice of a polycrystal. Therefore the expression for incoherent PBs in a polycrystal is given by the same formula (5.10) as in the case of a single-crystal target.

It should be noted that averaging by the formula (5.13) assumes that crystallites forming the polycrystal are of large enough size, so for each of them the expression for the structure factor of Eq. 5.3 is true.

After averaging the right side of the Eq. 5.8, with the use of Eq. 5.13 we obtain for the coherent component of PBs of a fast particle with the charge $Z_p\, e$ the following expression:

$$\left(\frac{dN}{d\omega\, d\Omega_k\, dx}\right)_{coh} = \frac{4\,\pi\, n_a^2\, Z_p^2\, e^2\, \omega^3}{\mathrm{v}^2\, c^3\, \hbar} \times$$
$$\times \sum_g N(g)\, \frac{\left|\alpha(\omega)\, \tilde{F}_a(g)\right|^2}{g^3}\, \exp\left(-g^2\, u^2\right)\, I_\varphi(g, \mathrm{v}, \omega, \theta)$$
$$\times\, \Theta\left(g\,\mathrm{v} - \omega\left(1 - \frac{\mathrm{v}}{c}\cos\theta\right)\right), \tag{5.14}$$

where $\Theta(x)$ is the Heaviside theta function that is equal to zero at a negative value of the argument and to one at a positive value. The theta function arose as a result of averaging over the solid angle $\mathbf{\Omega_g}$ of the delta function $\delta(\omega + \mathbf{gv} - \mathbf{kv})$ appearing in the expression (5.8). The kinematic integral $I_\varphi(g, \mathrm{v}, \omega, \theta)$ is given by the formulas (4.53), and in the nonrelativistic limit by the formula (4.53a). Introduced into the expression (5.14) is the charge number of an incident particle Z_p to describe PBs of a multiply charged ion, when $Z_p > 1$. It is obvious that in case of an electron $Z_p = -1$. Instead of summation over the reciprocal lattice vectors in the formula (5.8), on the right side of the Eq. 5.14 summation is carried out over the magnitudes of the reciprocal lattice vectors $g = |\mathbf{g}|$, $N(g)$ is the number of reciprocal crystal lattice vectors with a specified magnitude.

From the expression (5.14) it follows that in the spectrum of coherent PBs in a polycrystal spectral "steps" appear at frequencies defined by the magnitude of the reciprocal lattice vector g_j, by the velocity of an incident particle v and the radiation angle θ according to the equation:

$$\omega_j(\mathrm{v}, \theta) = \frac{g_j\, \mathrm{v}}{1 - \frac{\mathrm{v}}{c}\cos\theta} \tag{5.15}$$

Hence it is seen that in the nonrelativistic case $\mathrm{v} << c$ the frequency of the spectral step (Eq. 5.15) does not depend on the radiation angle and is directly proportional to the velocity of an incident particle.

An example of spectral steps in PBs on a polycrystalline target is presented in Fig. 5.3, in which the spectral dependence of PBs for scattering by a silver atom of an ion with the charge number $Z_p = 30$ and the velocity $\mathrm{v} = c/3$ is also given [3].

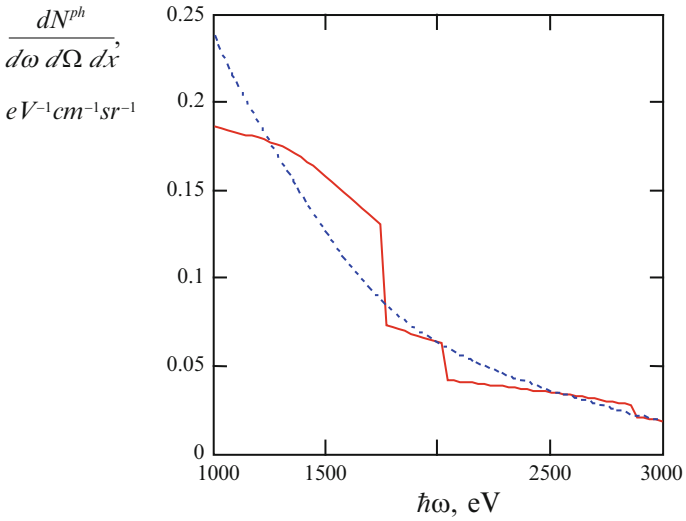

Fig. 5.3 PBs of a multiply charged ion in a silver polycrystal (*solid curve*) and on a silver atom (*dotted curve*)

For specified values of problem parameters (ion velocity and radiation angle), in the frequency range shown in Fig. 5.3 there are three frequency steps, the position of which is determined by the equation (5.15). For frequencies more than ω_j the contribution of the specified magnitude of the reciprocal lattice vector $\mathbf{g}$ to the process probability is equal to zero since the law of conservation of energy-momentum is not followed for it. As a result, a "frequency step" appears on the spectral dependence of yield of PBs photons. Since the frequency ω_j is defined by the magnitude of the vector $\mathbf{g}$, for which $S(\mathbf{g}) \neq 0$, the form of the spectrum of PBs in a polycrystal depends on the crystal structure of a target. For example, for a diamond-type crystal lattice the number of frequency steps will be less than for a face-centered lattice corresponding to silver. Really, in case of a diamond lattice there is an additional restriction for reciprocal lattice vectors, for which the structure factor of a unit cell is nonzero according to the formula (5.5).

The "manifestation" of the spectral step depends on the relation between the coherent and incoherent contributions to PBs. If incoherent PBs prevails, the frequency step will be "slurred over". To avoid this, the fulfilment of the condition is necessary:

$$g < \frac{1}{u}\left(1 - \frac{\mathrm{v}}{c}\cos\theta\right), \tag{5.16}$$

where u is the root-mean-square deviation of medium atoms from the equilibrium position. From the given inequation it follows that the stepped structure in the PBs spectrum for the specified magnitude of the reciprocal lattice vector will be more contrast for wide radiation angles θ. Really, with growing angle θ the minimum

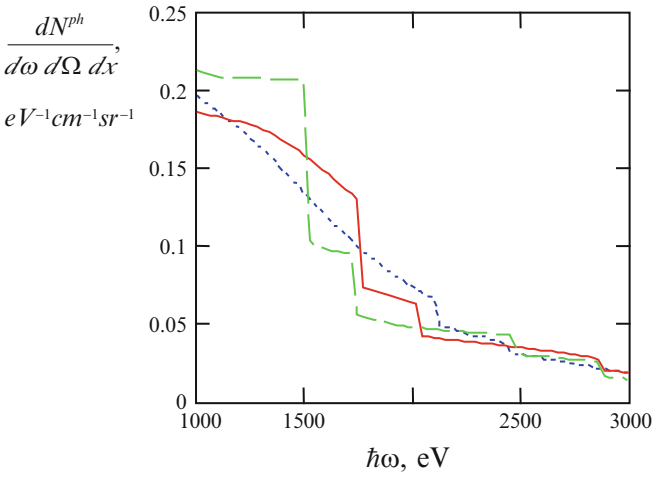

Fig. 5.4 The spectrum of PBs in a silver polycrystal for different radiation angles: *solid curve* – 90°, *dotted curve* – 60°, *dashed curve* – 120°

momentum transferred to a target increases and the contribution of the incoherent component of PBs decreases.

For reference we will give the formula for the root-mean-square deviation of crystal lattice atoms from their equilibrium position:

$$\langle u^2 \rangle = \frac{3\hbar^2}{4 M_a T_D} \left[1 + 4 \left(\frac{T}{T_D} \right)^2 \int_0^{T_D/T} \frac{y\, dy}{e^y - 1} \right], \tag{5.17}$$

where T_D is the Debye temperature in energy units, M_a is the mass of substance atoms. The Debye temperatures for aluminum, silicon, iron, and copper are respectively 418, 658, 467, and 339 K [1].

The dependence of the spectrum of PBs in a silver polycrystal on the angle of bremsstrahlung photon radiation is shown in Fig. 5.4.

From this figure it is seen that with increasing radiation angle the relative value of the "frequency jump" increases, and its position is shifted to the region of lower frequencies according to the formulas (5.15), and (5.16). Really, if the radiation angle is obtuse (the cosine is a negative value), then, as seen from the Eq. (5.16), the condition of "manifestation" of the spectral step is satisfied better than for smaller angles, when the cosine is equal to zero or takes on positive values. Physically this is connected with the fact that with growing radiation angle the relative contribution of the coherent component of PBs increases (in comparison with the incoherent component), and spectral steps, as seen from the expression (5.14), are caused just by coherent PBs. Thus the spectral steps are more noticeable for a radiation angle of 120° and are poorly discernible for a angle of 60°.

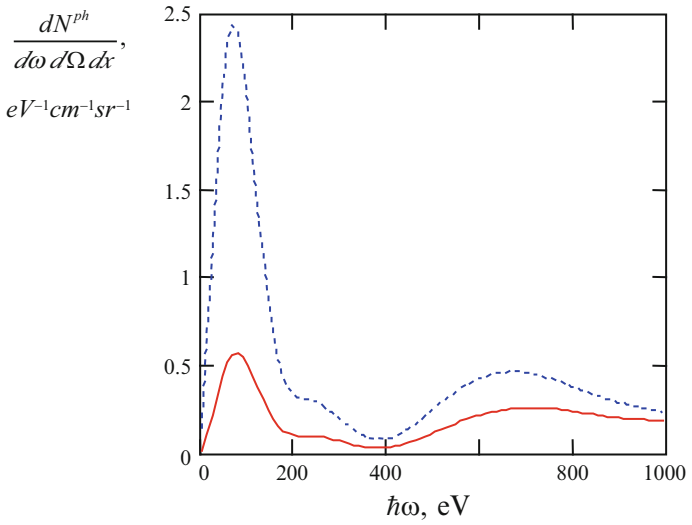

Fig. 5.5 PBs of an ion with the charge $Z_p = 30$ and the velocity $v = c/3$ in a silver polycrystal (*solid curve*) and on a silver atom (*dotted curve*) in the low-frequency range

In calculation of the spectrum of PBs in a silver polycrystal the following value of root-mean-square deviation of lattice ions from their equilibrium values $u_{Ag} = 0.087$Å was used. In the sum over the vectors of the reciprocal lattice with equal magnitudes that defines coherent PBs 50 summands were taken into account, for which $S(\mathbf{g}) \neq 0$. It should be noted that in taking into account 40 summands the result for photon yield (in an energy range from 1 to 10 keV) changes less than by 1 %.

Shown in Fig. 5.5 is the spectrum of PBs of a multiply charged ion $Z_p = 30$ with the velocity $v = c/3$ for a radiation angle of 90° in a silver polycrystal and on a silver atom in the low-frequency range.

In this case spectral steps are absent since the argument of the theta function in the formula (5.14) is positive for all $g \neq 0$. It is also seen that in this frequency range PBs in a polycrystal is *suppressed* in comparison with PBs on an isolated atom. This fact can be explained by superimposition of two circumstances. First, as seen from the formula (5.10), in the region of low frequencies $\omega < v/u$ the incoherent summand it small, and PBs is defined by the coherent component (Eq. 5.14). Second, momenta transferred to a target do not all make a contribution to coherent PBs in a polycrystal, but only those momenta, the magnitudes of which are equal to the magnitude of one of reciprocal lattice vectors. It is this fact that reduces the process intensity in comparison with radiation on an isolated atom, when the contribution to the process is made by all momenta transferred to a target that are permitted by the conservation law. For example, for the frequencies $\omega << v\, g$ the transferred momenta of small magnitude $\omega/v \leq q < g$ do not make a contribution to coherent PBs in a polycrystal, while it is just these momenta that play an important role in formation of PBs on an isolated atom.

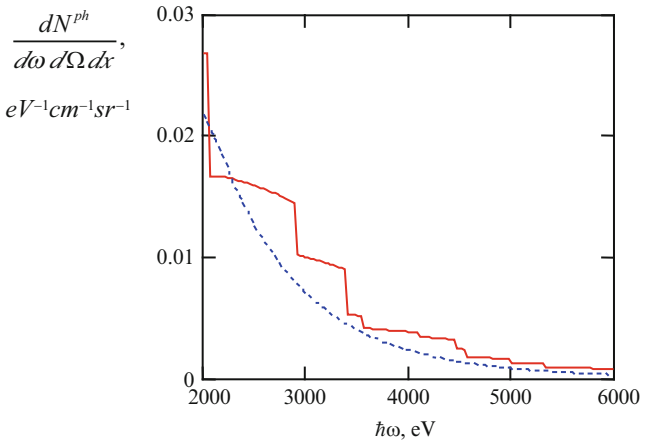

Fig. 5.6 The yield of PBs photons per unit trajectory length for an ion scattered in polycrystalline aluminum for different ion velocities: *solid curve* – v = c/3 (the ordinate is increased five times), *dotted curve* – v = c/20

The maxima of the frequency dependence in Fig. 5.5 are connected with the maxima of the imaginary part of the silver atom polarizability for photon energies close to the potentials of ionization of the shells *N* and *M*.

Presented in Fig. 5.6 is the dependence of the spectrum of PBs in an aluminum polycrystal on the velocity of an incident particle. The solid curve represents the radiation spectrum for a rather high value of the ion velocity (v = c/3).

With decreasing velocity, first, the contribution of the incoherent process increases, and second, the position of frequency steps is shifted to the low-frequency range.

Thus the position of a frequency step in the PBs spectrum can serve as a measure of energy of a scattered ion, and by the frequency shift ω_j it is possible to judge the energy loss for an incident particle. The dashed curve in Fig. 5.6 corresponds to the ion velocity equal to the velocity of protons with an energy of 1 MeV used in the experiments [4]. It is seen that in such an event the PBs spectrum does not contain a characteristic solid-state structure, but coincides with the spectrum of radiation on an isolated atom. It was this fact that took place in the experiments [4], in which no stepped spectrum structure was observed. This is explained by the fact that in case of low ion velocities the incoherent component of PBs prevails over the coherent component beginning with a photon energy of 500 eV. As a result, the stepped spectrum structure is found to be completely hidden behind the incoherent background.

Presented in Fig. 5.7 is the ratio of the contributions of the coherent and incoherent PBs channels for two values of energy (50 and 10 keV) of an electron scattered in polycrystalline copper, the radiation angle is 90°.

It will be recalled that coherent PBs corresponds to transfer of a momentum from an incident particle to a crystal lattice as a whole, and incoherent PBs arises during

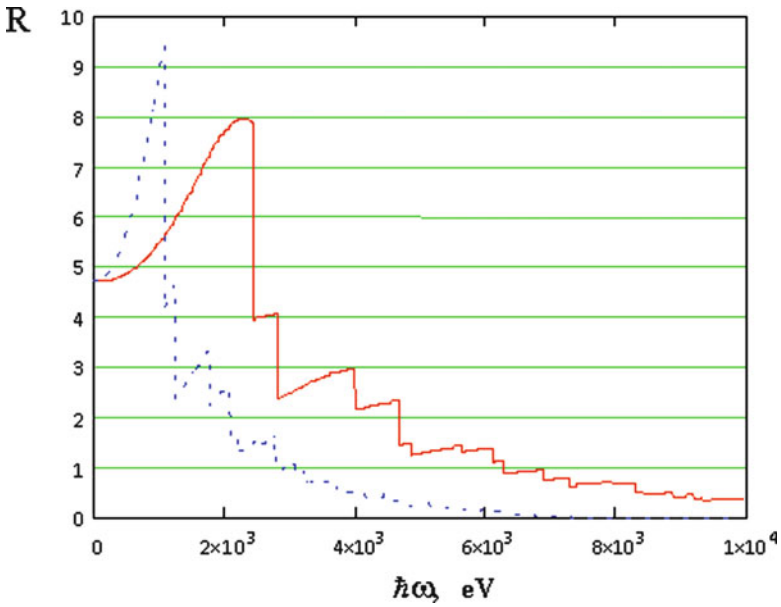

Fig. 5.7 The ratio of the coherent channel to the incoherent channel in PBs of an electron with an energy of 50 keV (*solid curve*) and 10 keV (*dash*-and-*dot curve*) scattered in copper

pair collisions between a scattered charge and target atoms. It is seen that in the low-frequency range coherent PBs prevails over incoherent PBs, for 50 keV electrons the contributions of both channels being compared at $\hbar\omega = 6.1$ keV and for 10 keV electrons at $\hbar\omega = 3$ keV. Thus the more is the velocity of an incident particle the wider is the spectral range of prevalence of coherent PBs over incoherent PBs.

In the high-frequency region of the PBs spectrum ($\hbar\omega > 10$ keV) characterized by high values of the momentum transferred to a target (or low values of the impact parameter) incoherent PBs prevails. Therefore the solid-state spectrum structure caused by the coherent interaction of an incident particle with the target becomes poorly discernible. As a result, the spectrum of PBs in a polycrystal approaches the spectrum on an isolated atom as it must be according to the physical picture of the process.

Thus for observation of frequency steps in the spectrum of PBs on a polycrystal it is necessary to use charged particles of high enough energy and to watch in the intermediate region of photon energy: from 1.5–2 to about 6 keV.

In the relativistic case in the PBs spectrum, instead of spectral steps, peaks are observed that correspond to the fulfilment of the Bragg condition for a virtual photon scattered by a polycrystalline target to a real photon. The maximum condition can be obtained from the formula (4.53) in the limit $\Delta \to 0$. Then we have $x_{\max} \approx 2\sin(\theta/2)$ or $\omega_g \approx g\,c/2\sin(\theta/2)$ – the frequency of a peak in the spectrum of PBs of a relativistic particle corresponding to the magnitude of the

reciprocal crystal lattice vector g. An analogous result was obtained in the N.N. Nasonov's work [5] within the framework of classical electrodynamics. Experimentally, the maxima of PBs of relativistic electrons in a polycrystalline target were for the first time recorded in the work [6] (see Fig. 2 of Chap. 1).

As was already said, the maxima in the spectrum of coherent PBs of a relativistic electron in a polycrystal correspond to Bragg scattering of virtual photons of its electromagnetic field by atomic planes. The Bragg condition for PBs in a polycrystal in the limit is expressed by the equation

$$\mathbf{k} - |\mathbf{k}| \frac{\mathbf{v}}{\mathrm{v}} = \mathbf{g}. \tag{5.18}$$

In writing Eq. 5.18 it was assumed that the wave vector of a virtual photon is directed along the velocity of an incident particle and is equal in magnitude to the wave vector of a real bremsstrahlung photon. This assumption is substantiated by the fact that the structure of the ultrarelativistic charge field is close to a plane wave with a wave vector parallel to the velocity of a particle. The graphic representation of the Eq. 5.18 is given in Fig. 5.8.

It should be noted that in case of a polycrystalline target for any radiation angle there will always be a crystallite, one of crystallographic planes of which is the bisector of the angle between the vectors **k** and **v** as shown in Fig. 5.8.

5.3 Polarization Bremsstrahlung in an Amorphous Medium

In case of PBs on an amorphous target, instead of the crystal structure factor (5.3) in the formula for the Bs cross-section (5.1) the following expression should be used:

$$S(\mathbf{q}) = {n_a}^{-1} \sum_{j,l} \left\langle \exp\left(i\,\mathbf{q}\,(\mathbf{r}_j - \mathbf{r}_l)\right)\right\rangle = 1 + n_a \int [g(r) - 1]\, \exp(i\,\mathbf{q}\,\mathbf{r})\, d\mathbf{r}. \tag{5.19}$$

The second equation in Eq. 5.19, where $g(r)$ is the pair correlation function for atoms, relates to an isotropic medium. For the structure factor of an amorphous substance in the "hard-sphere" approximation, when $g(r) = \Theta(r - D_a)$ (D_a is the mean diameter of an atom, $\Theta(x)$ is the theta function), from Eq. 5.19 it follows:

$$S_{amor}(q) = \left[1 - \sigma\, \frac{3 j_1(q D_a)}{q D_a}\right],\ \sigma = \frac{4\,\pi\, n_a {D_a}^3}{3}, \tag{5.20}$$

where $j_1(x)$ is the first-order spherical Bessel function. The second summand in the square brackets of the second equation (5.19) reflects the fact of destructive

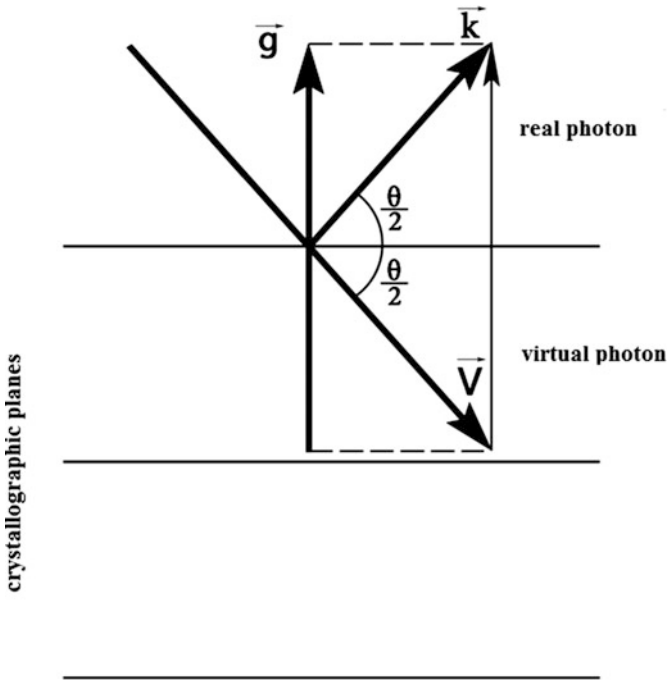

Fig. 5.8 The graphic representation of the Bragg condition for PBs of a relativistic particle scattered in a crystal

interference of the contributions of amorphous medium atoms to the total PBs intensity, with the result that the suppression of PBs occurs. It is obvious that the effect of PBs suppression connected with this interference is essential in the case that the parameter σ is close to one. Besides, for manifestation of this effect it is necessary that the argument of the spherical Bessel function $x = q D_a$ is less than one. Hence in view of the expression for the minimum momentum transferred to the medium $q_{\min} = (1 - (\mathrm{v}/\mathrm{c})\cos\theta)(\omega/\mathrm{v})$, we obtain:

$$\omega < \frac{\mathrm{v}}{D_a\,(1 - (\mathrm{v}/\tilde{c})\cos\theta)}, \tag{5.21}$$

where $\tilde{c}$ is the velocity of light in the target material. This inequation (with fulfilment of the condition $\sigma \approx 1$) determines the spectral range of suppression of PBs in an amorphous medium depending on the IP velocity and the angle of photon emission. Physically, corresponding to the condition (5.21) are such parameters of the problem, with which the contribution of small transferred momenta (high impact parameters) to the process is essential. Then PBs is of a collective nature, and mutual screening of different atoms reducing the process intensity occurs. This screening can be interpreted also as destructive interference of elementary PBs fields formed by individual atoms.

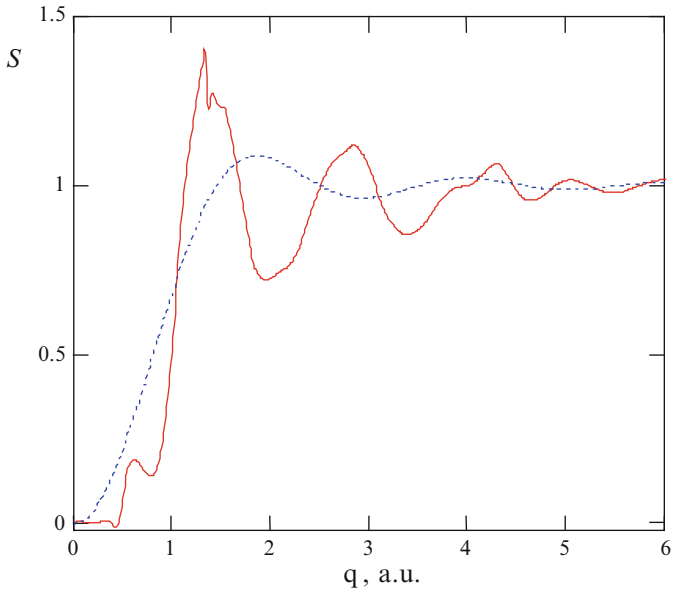

Fig. 5.9 The structure factor of amorphous silicon: *solid curve* – quantum-chemical calculation [7], *dotted curve* – calculation by the formula (5.20)

The use of the "hard-sphere" approximation (Eq. 5.20) for calculation of PBs intensity requires knowledge of the parameter $\sigma = 4\pi n_a D_a^3/3$. And if the concentration of atoms can be easily estimated from the known density of a substance, in determination of the mean atomic radius D_a being a model value there can be difficulties, especially in case of a medium with high atomic concentration. Let us illustrate the aforesaid by the example of the structure factor of liquid silicon, for which in the work [7] the results of quantum-chemical calculations are given. Calculated in [7], the dependence of the structure factor on the momentum transferred to the medium q at the melting temperature for silicon $T = 1410°\mathrm{C}$ is presented in Fig. 5.9 by the solid curve. Given in the same figure is the structure factor of liquid silicon calculated in the "hard-sphere" model for $\sigma = 1$ (dotted curve). This value of the parameter σ for the real density of liquid silicon $n_a = 5.446 \times 10^{22}$ cm^{-3} corresponds to the mean $D_a = 1.64$ Å that was used in construction of the dotted curve of Fig. 5.9. At the same time the tabular value of the silicon atomic diameter is $D_a = 2.36$ Å [8]. (It should be noted that the doubled Wigner-Seitz radius for the above concentration of silicon atoms is 3.27 Å). But with such a value of D_a the parameter $\sigma \cong 3$, so $S(q \to 0) < 0$, which is in contradiction with the positive definiteness of the structure factor of the medium.

A similar conclusion can be made for amorphous carbon and other condensed media of light atoms, when the model structure factor (5.20) causes a contradiction with the numerical values of the problem parameters. It should be noted that the pair

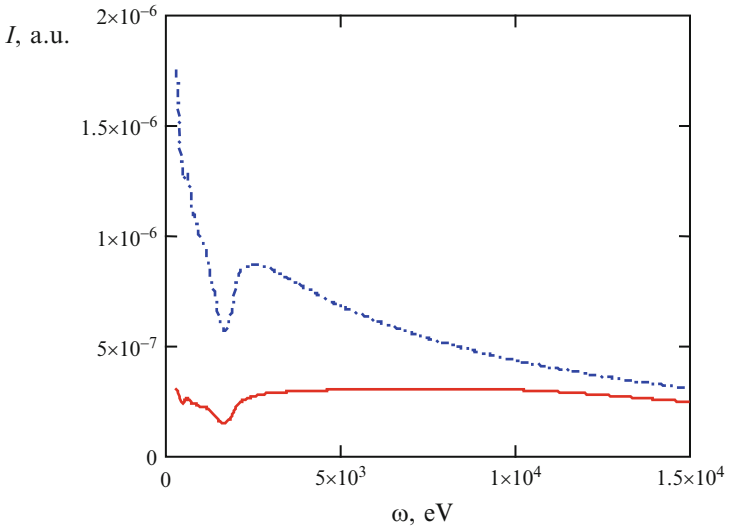

Fig. 5.10 The spectral intensity of PBs of an electron with $\gamma = 10$ on a target of amorphous silicon at the angle of radiation $\theta = 18°$: *solid curve* – radiation in amorphous silicon, *dash*-and-*dot curve* – PBs on an individual silicon atom

correlation function $g(r)$ used in the work [7] for determination of $S(q)$ differs noticeably from the theta function of the "hard-sphere" model. This difference is especially great at short distances $r \approx D_a$, where there is a maximum of the correlation function: $g \approx 2$. The last circumstance is indicative of the presence of a short-range order in liquid silicon at melting temperature.

Presented in Fig. 5.10 are the results of calculation of the spectrum of PBs in liquid silicon normalized to the concentration of medium atoms n_a and in scattering of an electron by an isolated atom. The plots of Fig. 5.10 are constructed for a relativistic electron with the Lorentz factor $\gamma = 10$ ($\gamma = \left(1 - (\mathrm{v}/c)^2\right)^{-1/2}$) and the angle of bremsstrahlung photon radiation $\theta = 18°$. The maximum of the spectral dependence for an isolated atom is caused by increasing polarization charge of a silicon atom, when the bremsstrahlung photon energy approaches the energy of ionization of the K-shell.

It is seen that the intensity of PBs in liquid silicon is much less than in the monatomic case throughout the range of photon energies due to destructive interference of contributions of different atoms discussed above. The calculation shows that for the larger radiation angle $\theta = 90°$ and the same other parameters the effect of PBs suppression takes place in the low-energy range $\hbar\,\omega < 3$ keV. This fact corresponds to the inequation (5.21) determining the region of essentiality of destructive interference in PBs. In the relativistic case with growing radiation angle the minimum momentum transferred to a medium increases and, as a result, the role of cooperative effects causing destructive interference decreases. Therefore

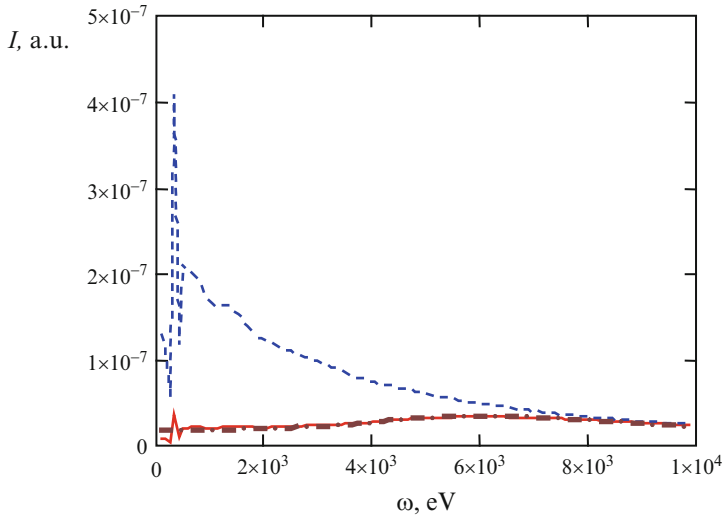

Fig. 5.11 The spectral intensity of PBs of a relativistic electron ($\gamma = 10$, $\theta = 45^\circ$) on a carbon target: *solid curve* – radiation on a target of amorphous carbon, *dotted curve* – PBs on a carbon atom, *dash*-and-*dot curve* – PBs on amorphous carbon in the high-frequency approximation

the effect of suppression of PBs intensity for large radiation angles occurs at lower frequencies, when the minimum transferred momentum is low enough, and in an elementary radiative act several medium atoms are involved.

In the experiment [9] that has shown the effect of suppression of PBs in an amorphous medium, radiation of an electron with an energy of 5–7 MeV scattered by a thin-film target of amorphous carbon was recorded. It is of interest to calculate the PBs intensity for experimental conditions [9] within the framework of the approach under consideration. The corresponding results are given in Fig. 5.11 for the Lorentz factor of a scattered electron $\gamma = 10$, the radiation angle 45°, the target density $\rho = 2.4$ g/cm^3, and the mean diameter of a carbon atom $D_a = 1.258$ Å, (at which $\sigma = 4\pi n_a D_a^3/3 = 1$).

Shown in the same figure are the results of calculation of the PBs intensity in amorphous carbon in the high-frequency approximation. From the form of the curves it follows that the suppression effect is most pronounced in the range of bremsstrahlung photon energies $\hbar\omega < 5$ keV, which corresponds to the experimental data of the work [9]. The maxima of the spectral dependences correspond to the binding energies for electrons of the K – and L-shells of a carbon atom – 296 and 16.6 eV. It is seen also that the high-frequency approximation well describes the process in a wide spectral range up to photon energies of 300 eV.

The analysis shows that the error of calculation of PBs intensity caused by inaccuracy of the model used for the structure factor of a medium depends on problem parameters. This error is most essential in the low-frequency range for large radiation angles, besides, it grows with increasing energy of an incident electron. The comparison of the results of calculation of PBs in liquid silicon

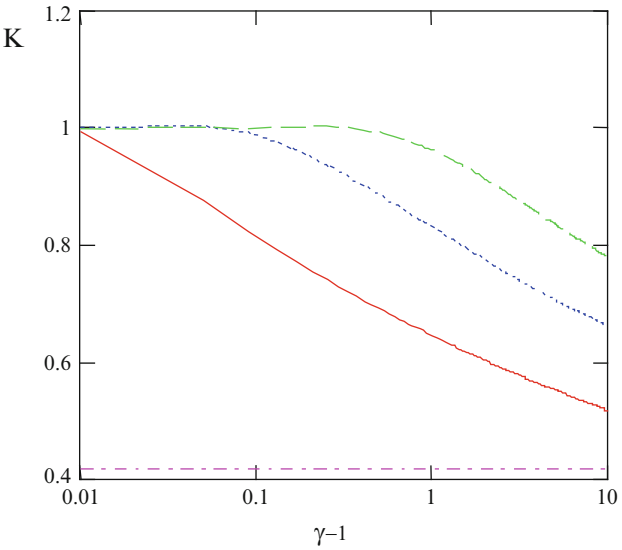

Fig. 5.12 The suppression ratio for PBs in amorphous silver as a function of the energy of an incident particle for the radiation angle $\theta = 18°$ and three values of bremsstrahlung photon energy: *solid curve* –$\hbar\omega = 300$ eV, *dotted curve* – $\hbar\omega = 1$ keV, *dashed curve* – $\hbar\omega = 3$ keV

obtained in the "hard-sphere" model and with the use of the quantum-chemical structure factor [7] gives a characteristic error no more than 20 % for $\gamma = 10$ and $\theta = 18°$. With growing radiation angle the calculation error increases, but the effect of PBs suppression itself decreases.

The effect of suppression of PBs in an amorphous medium in the X-ray range is essential only for relativistic incident particles. In case of a nonrelativistic electron beam it can be neglected, at least for bremsstrahlung photon energies more than 1 keV. This circumstance is illustrated by Fig. 5.12, where the X-axis corresponds to the energy of an incident particle normalized to the rest energy (for an electron to 511 keV), the Y-axis is the ratio of the intensity of PBs in an amorphous medium to the intensity of PBs on an atom.

Also shown in Fig. 5.12 is the straight line corresponding to the value of the PBs suppression ratio obtained in the limit of low transferred momenta: $K = 1 - \sigma = 0.417$. The suppression effect more strongly shows itself for lower photon energies, when the role of destructive interference of contributions of different atoms to the intensity of the process is great. In the low-frequency range PBs suppression occurs also for nonrelativistic incident particles, when $\gamma - 1 << 1$. For photons of high energies ($\omega > 1$ keV) the PBs intensity decreases noticeably only in case of high Lorentz factors γ. A characteristic feature of the curves in Fig. 5.12 is the presence of such inflection points γ^* that for $\gamma > \gamma^*$ the effect of PBs suppression begins. It should be noted that for large values of the Lorentz factor $\gamma > 10^4$ the suppression ratio becomes less than its limiting value $K = 1 - \sigma = 0.417$ (calculated to the logarithmic accuracy). This is connected with the density

effect in PBs, when the intensity of the process decreases as a result of screening of the IP eigenfield at $\varepsilon(\omega) < 1$ ($\varepsilon(\omega)$ is the dielectric permittivity of a medium). The last inequation for a silver target is satisfied in the range of photon energies: $\hbar\,\omega > 50$ eV.

A similar effect of suppression of PBs intensity in the low-frequency range takes place in scattering of a charged incident particle in a polycrystal [3] as was said in the previous section. As in case of an amorphous medium in a polycrystal for low transferred momenta $q < 2\,\pi/d$ (d is the lattice constant), the interference of the contributions of substance atoms to the intensity of the polarization channel is of a destructive nature, reducing the intensity of radiation. It should be noted that the appreciable value of the suppression ratio in an amorphous medium is possible only for relativistic incident particles (Fig. 5.12), while in a polycrystal the PBs intensity considerably decreases (times) in comparison with an isolated atom and in the nonrelativistic case [3].

The obtained expressions for the cross-section of Bs in different solid-state targets can be also used for estimation of intensity of radiation of secondary electrons produced in the target material by a primary electron beam, with corresponding replacement of kinematic parameters (velocity, photon energy, and radiation angle).

References

1. Ter-Mikaelian, M.: High Energy Electromagnetic Processes in Condensed Media. Wiley, New York (1972)
2. Animalu, A.O.E.: Intermediate Quantum Theory of Crystalline Solids. Prentice-Hall, New Jersey (1978)
3. Astapenko, V.A.: Polarization bremsstrahlung of heavy charged particles in polycrystal. JETP **99**, 958 (2004)
4. Ishii, K., Morita, S.: Continuum x-ray produced by light-ion-atom collisions. Phys. Rev. A **30**, 2278 (1984)
5. Nasonov, N.N.: Collective effects in the polarization bremsstrahlung of relativistic electrons in condensed media. NIM B **145**, 19 (1998)
6. Blashevich, S., Chepurnov, A., Grishin, V., et al.: Polarization bremsstrahlung of relativistic electrons in aluminium. Phys. Lett. A **254**, 230 (1999)
7. Stillinger, F.H., Weber, T.A.: Computer simulation of local order in condensed phases of silicon. Phys. Rev. B **31**, 5262 (1985)
8. Grigoriev, I.S., Meilihov, E.Z: Fisicheskie velichiny. Energoatomizdat, Moscow (1991) (in Russian)
9. Blashevich, S.V., Chepurnov, A.S., Grishin, V.K., et al.: Suppression of polarization bremsstrahlung of relativistic electrons moving through an amorphous carbon foil. Phys. Lett. A **211**, 309 (1996)